

Discrete Breathers and Multi-Breathers in Finite Vibro-Impact Chain

Itay Grinberg^{1,*} and Oleg V. Gendelman^{1,†}

¹*Faculty of Mechanical Engineering
Technion - Israel Institute of Technology*

(Dated: September 21, 2018)

We explore dynamics of discrete breathers and multi-breathers in finite one-dimensional chain. The model involves parabolic on-site potential with rigid constraints and linear nearest-neighbor coupling. The rigid non-ideal impact constraints are the only source of nonlinearity and damping in the model. The model allows derivation of exact analytic solutions for the breathers and multi-breathers with arbitrary set of localization sites, both in conservative and forced-damped settings. We choose periodic boundary conditions; exact solutions for other types of the boundary conditions are also possible. Local character of the nonlinearity allows explicit derivation of a monodromy matrix for the breather solutions. Consequently, a stability of the derived breather and multi-breather solutions can be efficiently studied in the framework of simple methods of linear algebra, and with rather moderate computational efforts. We demonstrate that finiteness of the chain fragment and proximity of the localization sites strongly effect existence and stability patterns of these localized solutions.

PACS numbers 05.45.Yv, 63.20.Pw, 63.20.Ry

I. INTRODUCTION

Localization is a well-known phenomenon in nonlinear lattices [1–8]. Remarkable example of such localized dynamic states are discrete breathers (DBs), sometimes referred to as intrinsic localized modes (ILM) or discrete solitons. In lattices with linear coupling, the DBs are localized exponentially; if the coupling is strongly nonlinear, the localization may become hyper-exponential [2]. The DBs were experimentally observed and explored in many physical systems, including, among others, superconducting Josephson junctions[9], nonlinear magnetic metamaterials[10], electrical lattices[11], micro-mechanical cantilever arrays[12–16], Bose-Einstein condensates[17], and chains of mechanical oscillators[18–20].

Theoretical investigation of the DBs relied primarily on numeric and approximate analytic methods[1, 2]. Exact analytic solutions for the DBs are quite scarce, due to combination of discreteness and non-linearity. Known exceptions are completely integrable Ablowitz-Ladik model[21] and chain with homogeneous interactions[22]. Recently this family has been extended by derivation of analytic solutions for the DBs in conservative vibro-impact chains [18]. The vibro-impact chains also allowed computation of the exact solutions for forced-damped discrete breathers [20, 23].

In these latter works, one important peculiarity of the vibro-impact models has been explored and used. If all interactions besides the collisions with the impact constraints are considered to be linear, then it is possible to drastically simplify the analysis of stability for the DB solutions. The DBs are periodic solutions of a system

of ordinary differential equations, and their stability is determined by the location of eigenvalues of the monodromy matrix, computed for the DB solution in the given system[24]. Commonly the monodromy matrix has to be computed numerically, by integration of the system with N degrees of freedom over the period, with $2N$ different initial conditions for every point in the space of parameters. For systems large enough, such task is amenable only by supercomputers. For the vibro-impact models mentioned above, the monodromy matrix can be explicitly expressed in a general form[20, 23], and the numeric part is reduced to relatively rapid and simple computation of the eigenvalues of this matrix for given parameter values. This simplification allows detailed exploration of the stability patterns in the space of parameters for the DB solutions.

Current work is based on the approaches developed in [18, 20, 23], and extends them in two aspects. First of all, all experimental setups mentioned above include finite (and sometimes rather small) number of coupled oscillatory systems. From the other side, it is possible to excite more than one site of the lattice, and these excited sites are not necessarily adjacent. Thus, one can observe and explore the multi-breather (MB) solutions. The existing knowledge on properties and especially on the stability of the MBs is rather limited. Due to its simplicity, the vibro-impact model seems natural for derivation and exploration of the MB solutions in finite systems. The paper addresses exactly this problem. In Section II we describe the general model settings. In Section III the exact solutions for the multi-breathers both in Hamiltonian and forced-damped settings are derived. Section IV investigates the stability properties of the obtained solutions. Section V presents numeric validation and illustrations of the results of the previous Sections. Section VI adds some concluding remarks.

*Electronic address: GrinbergItay@gmail.com

†Electronic address: ovgend@technion.ac.il

II. DESCRIPTION OF THE MODEL

We consider a finite chain of identical unit masses, coupled with linear springs, and with periodic boundary conditions. Besides, each mass has the same on-site interaction – a linear spring with symmetric pair of impact barriers located at distances $u_n = \pm 1$ from the trivial equilibrium position. This unit scaling does not restrict the generality. The Hamiltonian of the systems that includes $(N + 1)$ masses is written as follows:

$$H = \sum_{n=0}^N \left(\frac{1}{2} p_n^2 + V(u_n) \right) + \sum_{n=0}^{N-1} W(u_n - u_{n+1}) + W(u_N - u_0) \quad (1)$$

$$V(x) = \begin{cases} \frac{\gamma_1}{2} x^2 & |x| < 1 \\ \text{infinity} & |x| = 1 \end{cases} \quad (2)$$

$$W(x) = \frac{\gamma_2}{2} x^2 \quad (3)$$

where $p_n = \dot{u}_n$ is the momentum of each particle, γ_1 and γ_2 are the on-site and coupling stiffnesses respectively and $V(x)$ and $W(x)$ are the on-site and coupling potentials respectively.

This yields the following linear equations of motion between the impacts, i.e. for $|u_n| < 1$ for all particles:

$$\ddot{u}_0 + \gamma_1 u_0 + \gamma_2 (2u_0 - u_1 - u_N) = 0 \quad (4)$$

$$\ddot{u}_n + \gamma_1 u_n + \gamma_2 (2u_n - u_{k+1} - u_{k-1}) = 0 \quad (5)$$

$$\ddot{u}_N + \gamma_1 u_N + \gamma_2 (2u_N - u_0 - u_{N-1}) = 0 \quad (6)$$

We adopt here traditional Newtonian model of the inelastic impacts. Namely, when at certain time instance $t = t_b$ some particle achieves the impact barrier ($u_n(t_b) = \pm 1$), its velocity is instantaneously modified according to the following law:

$$\dot{u}_n(t_b+) = -e \dot{u}_n(t_b-) \quad (7)$$

Here $0 < e \leq 1$ is a restitution coefficient.

III. EXACT SOLUTIONS FOR THE MULTI-BREATHERS

A. Hamiltonian Model

Let us proceed with analytic solution for the multi-breathers in the vibro-impact chain fragment described in the previous section. First, we are going to consider the conservative case, where $e = 1$ and no external force is applied. In the most generic setting, the multi-breather solution in this system corresponds to periodic oscillatory state, in which certain subset of masses periodically impacts the barriers, and the others do not achieve them. Without loss of generality, we suggest that the particle

with $n = 0$ is engaged in the impacts and the particle with $n = N$ does not impact the constraints. Every single impact may be presented as a result of action of the external force in the form of delta-function. We also suggest that all impacting masses undergo the impacts simultaneously. It is possible that some masses impact their right barriers, and the others impact their left barriers at the same time instance. Taking into account the periodicity of the MB solution, the latter should obey the following system of equations:

$$\ddot{u}_0 + \gamma_1 u_0 + \gamma_2 (2u_0 - u_1 - u_N) = 2p_0 \delta_0 \sum_{j=-\infty}^{\infty} \left(\delta \left(t - \frac{\pi(2j+1)}{\omega} \right) - \delta \left(t - \frac{2\pi j}{\omega} \right) \right) \quad (8)$$

$$\ddot{u}_n + \gamma_1 u_n + \gamma_2 (2u_n - u_{k+1} - u_{k-1}) = 2p_k \delta_{nk} \sum_{j=-\infty}^{\infty} \left(\delta \left(t - \frac{\pi(2j+1)}{\omega} \right) - \delta \left(t - \frac{2\pi j}{\omega} \right) \right) \quad (9)$$

$$\ddot{u}_N + \gamma_1 u_N + \gamma_2 (2u_N - u_0 - u_{N-1}) = 0 \quad (10)$$

where δ_{nk} is Kronecker delta, $\delta(t)$ is Dirak delta function, $k \in \{0, m_1, m_2, \dots, m_L\}$, m_l are the indices of the impacting masses, $L + 1$ is a number of impacting particles, and $2p_k$ is an amount of momentum transferred to the k -th particle by the impact constraint at the instance of the impact. ω is a fundamental frequency of the breather ($T = 2\pi/\omega$ is a minimal period). For the conservative model, $|p_k|$ is also the magnitude of the velocity of the impacting mass before and after the impact, due to the unit restitution coefficient.

The periodicity of the impacts allows us to rewrite equations (8)-(10) in terms of generalized Fourier series:

$$\ddot{u}_0 + \gamma_1 u_0 + \gamma_2 (2u_0 - u_1 - u_N) = -\frac{4\omega p_0 \delta_0 k}{\pi} \sum_{j=0}^{\infty} \cos((2j+1)\omega t) \quad (11)$$

$$\ddot{u}_n + \gamma_1 u_n + \gamma_2 (2u_n - u_{n+1} - u_{n-1}) = -\frac{4\omega p_k \delta_{nk}}{\pi} \sum_{j=0}^{\infty} \cos((2j+1)\omega t) \quad (12)$$

$$\ddot{u}_N + \gamma_1 u_N + \gamma_2 (2u_N - u_0 - u_{N-1}) = 0 \quad (13)$$

Heterogeneous solutions of equations (11)-(13) is presented in the following form of Fourier series:

$$u_n = \sum_{j=0}^{\infty} u_{n,j} \cos((2j+1)\omega t) \quad (14)$$

Furthermore, since the solution should be localized, the following anzats for $u_{n,j}$ is used:

$$u_{n,j} = \sum_k \left(A_{j,k} f_j^{|n-k|} + B_{j,k} f_j^{-|n-k|} \right) \quad (15)$$

Physically, this form of solution corresponds to the exponential localization around each breather site. System (11)-(13) between the impact time instances is linear and solutions for coefficients f_i should obey the following relationships:

$$\begin{aligned}
f_j &= \frac{\gamma_1 + 2\gamma_2 - (2j+1)^2 \omega^2 \pm \sqrt{\left((2j+1)^2 \omega^2 - \gamma_1 - 2\gamma_2\right)^2 - 4\gamma_2^2}}{2\gamma_2} = \\
&= \frac{\gamma_1 + 2\gamma_2 - (2j+1)^2 \omega^2 \pm \sqrt{\left((2j+1)^2 \omega^2 - \gamma_1 - 4\gamma_2\right) \left((2j+1)^2 \omega^2 - \gamma_1\right)}}{2\gamma_2}
\end{aligned} \tag{16}$$

In order to make spatial localization possible, the term under the square root should be positive – in other terms, the Hamiltonian DB exists only in the attenuation zone of the chain. As for the choice of the \pm sign - it is easy to see that inversion of the sign does not modify the solution. Relation between the coefficients $A_{j,k}$ and $B_{j,k}$ can be obtained from the periodic boundary conditions by substituting (15) in (13):

$$A_{j,k} = B_{j,k} f_j^{-N-1} \tag{17}$$

It is important to note here that $A_{j,k} = 0$ as $N \rightarrow \infty$ and the solution converges to that of the infinite chain [18].

Finally, for the impacting masses one obtains :

$$B_{j,k} = \frac{4\omega p_k}{\pi\gamma_2 (f_j - f_j^{-1}) (f_j^{-N-1} - 1)} \tag{18}$$

Thus, the solution for the chain fragment with the MB is expressed in the following form:

$$u_n = \sum_{j=0}^{\infty} u_{n,j} \cos((2j+1)\omega t) \tag{19}$$

where

$$u_{n,j} = \sum_k \frac{4\omega p_k \left(f_j^{|n-k|-N-1} + f_j^{-|n-k|} \right)}{\pi\gamma_2 (f_j - f_j^{-1}) (f_j^{-N-1} - 1)} \tag{20}$$

The only remaining unknown is the amount of momentum transferred in the course of each impact, i.e. p_k . It can be computed, if one takes into account the location of the barriers. Let $n = k_s$ be some impacting particle; then, at the instance of the impact one obtains:

$$u_{k_s}(0) = \sum_k \frac{4\omega p_k}{\pi\gamma_2} \chi_{k_s,k} = \pm 1 \tag{21}$$

where the \pm sign determines whether the specific mass is in-phase or out-of-phase with respect to the other impacting masses and,

$$\chi_{k_s,k} = \sum_{j=0}^{\infty} \frac{\left(f_j^{|k_s-k|-N-1} + f_j^{-|k_s-k|} \right)}{(f_j - f_j^{-1}) (f_j^{-N-1} - 1)} \tag{22}$$

Note that if the location of the impacting mass k_s at $t = 0$ is -1 , one should obtain $p_{k_s} < 0$ and vice versa.

The obtained set of equations can also be written in the following more compact form:

$$\begin{bmatrix} p_0 \\ p_{k_1} \\ \vdots \\ p_{k_m} \end{bmatrix} = \frac{\pi\gamma_2}{4\omega} \mathbf{C}^{-1} \begin{bmatrix} 1 \\ 1 \\ \vdots \\ 1 \end{bmatrix} \tag{23}$$

where $(m+1) \geq N$ is the number of impacting masses and:

$$\mathbf{C} = \begin{bmatrix} \chi_{0,0} & \chi_{0,k_1} & \cdots & \chi_{0,k_M} \\ \chi_{k_1,k_1} & \chi_{k_1,k_1} & & \vdots \\ \vdots & & \ddots & \vdots \\ \chi_{k_M,0} & \cdots & \cdots & \chi_{k_M,k_M} \end{bmatrix} \tag{24}$$

It is important to mention here that the self-consistency of the obtained solution (i.e. the fact that the particles, which are not selected as the ‘‘impacting’’ ones, indeed do not achieve the constraints) is difficult to prove analytically due to the complexity of the equations; it is explored numerically in section V. However, it is easy to see that as $N \rightarrow \infty$ there is exponential localization with respect to the localization sites, if they are concentrated at some finite sub-fragment of the chain.

B. Forced-Damped Model

In this case the model is slightly altered, since all masses are subjected to the same external force $F(t)$. We consider symmetric periodic external force $F(t)$ which satisfies $F(t) = F(t + \frac{2\pi}{\omega})$ and $F(t) = -F(t + \frac{\pi}{\omega})$. Additionally, the damping is introduced through the non-unit restitution coefficient $0 < e < 1$. Similarly to the Hamiltonian case, we look for the periodic solution, thus the impacts can be taken into account in the same form as above. The solution should obey the following set of equations:

$$\ddot{v}_0 + \gamma_1 v_0 + \gamma_2 (2v_0 - v_1 - v_N) = F(t) + 2p_0 \delta_{0k} \sum_{j=-\infty}^{\infty} \begin{pmatrix} \delta\left(t - \phi_0 - \frac{\pi(2j+1)}{\omega}\right) \\ -\delta\left(t - \phi_0 - \frac{2\pi j}{\omega}\right) \end{pmatrix} \quad (25)$$

$$\ddot{v}_n + \gamma_1 v_n + \gamma_2 (2v_n - v_{n+1} - v_{n-1}) = F(t) + 2p_k \delta_{nk} \sum_{j=-\infty}^{\infty} \begin{pmatrix} \delta\left(t - \phi_k - \frac{\pi(2j+1)}{\omega}\right) \\ -\delta\left(t - \phi_k - \frac{2\pi j}{\omega}\right) \end{pmatrix} \quad (26)$$

$$\ddot{v}_N + \gamma_1 v_N + \gamma_2 (2v_N - v_0 - v_{N-1}) = F(t) \quad (27)$$

where ϕ_k is the phase of the k -th particle with respect to the external force $F(t)$.

The external force $F(t)$ can be removed from the equations with the help of a simple transformation. Let $v_n(t) = u_n(t) + G(t)$ where $\ddot{G}(t) + \gamma_1 G(t) = F(t)$. Substitution into the above equations yields:

$$\ddot{u}_0 + \gamma_1 u_0 + \gamma_2 (2u_0 - u_1 - u_N) = 2p_0 \delta_{0k} \sum_{j=-\infty}^{\infty} \begin{pmatrix} \delta\left(t - \phi_0 - \frac{\pi(2j+1)}{\omega}\right) \\ -\delta\left(t - \phi_0 - \frac{2\pi j}{\omega}\right) \end{pmatrix} \quad (28)$$

$$\ddot{u}_n + \gamma_1 u_n + \gamma_2 (2u_n - u_{n+1} - u_{n-1}) = 2p_k \delta_{nk} \sum_{j=-\infty}^{\infty} \begin{pmatrix} \delta\left(t - \phi_k - \frac{\pi(2j+1)}{\omega}\right) \\ -\delta\left(t - \phi_k - \frac{2\pi j}{\omega}\right) \end{pmatrix} \quad (29)$$

$$\ddot{u}_N + \gamma_1 u_N + \gamma_2 (2u_N - u_0 - u_{N-1}) = 0 \quad (30)$$

One can observe that the above equations are identical to those of the Hamiltonian model, and therefore can be solved in a similar manner. Replacing the impact terms with appropriate generalized Fourier series yields:

$$\ddot{u}_0 + \gamma_1 u_0 + \gamma_2 (2u_0 - u_1 - u_N) = -\frac{4\omega p_0 \delta_{0k}}{\pi} \sum_{j=0}^{\infty} \cos((2j+1)\omega(t - \phi_0)) \quad (31)$$

$$\ddot{u}_n + \gamma_1 u_n + \gamma_2 (2u_n - u_{n+1} - u_{n-1}) = -\frac{4\omega p_k \delta_{nk}}{\pi} \sum_{j=0}^{\infty} \cos((2j+1)\omega(t - \phi_k)) \quad (32)$$

$$\ddot{u}_N + \gamma_1 u_N + \gamma_2 (2u_N - u_0 - u_{N-1}) = 0 \quad (33)$$

The ansatz has to be somewhat modified due to the phase differences:

$$u_n = \sum_k \sum_{j=0}^{\infty} u_{n,j,k} \cos((2j+1)\omega(t - \phi_k)) \quad (34)$$

where $u_{n,j,k}$ is derived in a way similar to the Hamiltonian case:

$$u_{n,j,k} = \frac{4\omega p_k}{\pi \gamma_2 (f_j - f_j^{-1}) (f_j^{-N-1} - 1)} \times \left(f_j^{|n-k|-N-1} + f_j^{-|n-k|} \right) \quad (35)$$

Unlike the Hamiltonian model, we have here two sets of unknowns - p_k and ϕ_k . Therefore, additional set of equations is required. The first set is derived from the

location of the barriers, as in the Hamiltonian case. The mass $k_s \in k$ hits the right barrier at $t = \phi_{k_s}$:

$$v_{k_s}(\phi_{k_s}) = \sum_k \frac{4\omega p_k}{\pi \gamma_2} \sum_{j=0}^{\infty} \frac{(f_j^{|k_s-k|-N-1} + f_j^{-|k_s-k|})}{(f_j - f_j^{-1}) (f_j^{-N-1} - 1)} \times \cos((2j+1)\omega(\phi_{k_s} - \phi_k)) + G(\phi_{k_s}) = 1 \quad (36)$$

In terms of the transformed variables, i.e. in terms of u_n , the impacts should be symmetrical; therefore, one obtains $\dot{u}(\phi_k^-) = -\dot{u}(\phi_k^+) = p_k$. However, in terms of the initial variables, the impact conditions (7) with the non-unit restitution coefficient should be satisfied. Thus, one obtains the second set of equations:

$$\begin{aligned} \dot{v}(\phi_k^+) &= \dot{u}(\phi_k^+) + \dot{G}(\phi_k) = \\ &= -p_k + \dot{G}(\phi_k) = -e \left(p_k + \dot{G}(\phi_k) \right) = \\ &= -e \left(\dot{u}(\phi_k^-) + \dot{G}(\phi_k) \right) = -e \dot{v}(\phi_k^-) \end{aligned} \quad (37)$$

$$\dot{G}(\phi_{k_s}) = q p_{k_s} \quad (38)$$

where $q = \frac{1-e}{1+e}$. Final set of equations for the unknown parameters of multi-breather solution is written as:

$$\begin{aligned} G(\phi_{k_s}) &= 1 - \\ &- \sum_k \frac{4\omega p_k}{\pi \gamma_2} \sum_{j=0}^{\infty} \frac{(f_j^{|k_s-k|-N-1} + f_j^{-|k_s-k|})}{(f_j - f_j^{-1}) (f_j^{-N-1} - 1)} \times \\ &\quad \times \cos((2j+1)\omega(\phi_{k_s} - \phi_k)) \end{aligned} \quad (39)$$

$$\dot{G}(\phi_{k_s}) = q p_{k_s} \quad (40)$$

Note that ϕ_k appears in the equations in a way that does not allow exact solution. So, additional simplifications or numeric approaches are required after this point.

1. In-Phase DBs

Simplification of equation (39) is possible, if one considers the multi-breather with all particles having the same phase with respect to the external forcing. This is a special case $\phi_k = \phi$. With this assumption, equations (39) become much simpler, since ϕ vanishes from the summations and equations (39)-(40) are reduced to the following form:

$$G(\phi) = 1 - \sum_k \frac{4\omega p_k}{\pi \gamma_2} \chi_{k_s,k} \quad (41)$$

$$\dot{G}(\phi) = q p_{k_s} \quad (42)$$

The second equation demands that $p_k = p$. Furthermore, the first equation then gives $\sum_k \chi_{k_s,k} \equiv \sigma$ regardless of k_s which means that the two sets of equations are independent of k_s . This leads to two conclusions. The first is that we only have to solve a set of two equations. The

second one is that the forced in-phase DBs are only possible when certain symmetries are satisfied – in order for $\sum_k \chi_{k_s, k}$ to be the same for any k_s , the proximity of each localization site to all other sites should be the same for all sites. For 2-site DB this is always true; however, for 3 and more sites this is only true if they are equally spaced, with account of the periodic boundary conditions.

Simple choice of harmonic forcing $F = A \cos(\omega t)$ yields:

$$G(t) = \tilde{A} \cos(\omega t) \quad (43)$$

where $\tilde{A} = -\frac{A}{\omega^2 - \gamma_1}$.

Substitution of (41) and (42) then leads to the following system of equations:

$$\tilde{A} \cos(\omega \phi) = 1 - \frac{4\omega p}{\pi \gamma_2} \sigma \quad (44)$$

$$-\tilde{A} \omega \sin(\omega \phi) = qp \quad (45)$$

Possible values of p are easily obtained:

$$p = \frac{4\pi \gamma_2 \omega^3 \sigma \pm \pi \gamma_2 \omega \sqrt{(4\omega^2 \sigma)^2 \tilde{A}^2 + (\pi \gamma_2 q)^2 (1 - \tilde{A}^2)}}{\left((4\omega^2 \sigma)^2 + (q\pi \gamma_2)^2 \right)} \quad (46)$$

This solution can be plugged back into equations (44)-(45) to determine which of them is physically meaningful, and to obtain the value of ϕ .

IV. STABILITY

The stability of the periodic multi-breather solutions will be investigated with the help of Floquet theory[24]. The Floquet multipliers are often evaluated numerically, but as mentioned in the introduction, the explored model allows explicit construction of the monodromy matrix. Then, it is easy to find its eigenvalues for every set of parameters; thus, broad regions of the parameter space can be explored for various structures of the breathers, and with limited numeric efforts. Moreover, the eigenvectors corresponding to the unstable Floquet multipliers can be easily computed and examined to give a qualitative insight into physical mechanisms of the loss of stability.

The governing equations of motion for Hamiltonian model can be re-written in the following equivalent form:

$$\dot{\vec{u}} = A \vec{u} \quad (47)$$

where $\vec{u} = [u_0 \cdots u_N \dot{u}_0 \cdots \dot{u}_N]^T$ and:

$$A = \begin{bmatrix} 0_{(N+1) \times (N+1)} & \mathbf{I}_{(N+1) \times (N+1)} \\ \tilde{A}_{(N+1) \times (N+1)} & 0_{(N+1) \times (N+1)} \end{bmatrix} \quad (48)$$

$$\tilde{A} = \begin{bmatrix} \gamma_1 + 2\gamma_2 & -\gamma_2 & 0 & \cdots & 0 & -\gamma_2 \\ -\gamma_2 & \gamma_1 + 2\gamma_2 & -\gamma_2 & 0 & \cdots & 0 \\ 0 & -\gamma_2 & \ddots & \ddots & \ddots & \vdots \\ \vdots & \ddots & \ddots & \gamma_1 + 2\gamma_2 & -\gamma_2 & 0 \\ 0 & \cdots & 0 & -\gamma_2 & \gamma_1 + 2\gamma_2 & -\gamma_2 \\ -\gamma_2 & 0 & \cdots & 0 & -\gamma_2 & \gamma_1 + 2\gamma_2 \end{bmatrix} \quad (49)$$

Here \tilde{A} is Laplace adjacency matrix of the system. For the forced-damped model, minor modification is required:

$$\dot{\vec{v}} = A \vec{v} + \vec{F} \quad (50)$$

where $\vec{F} = F(t) [0 \cdots 0 \ 1 \cdots 1]^T$.

All considered solutions, both for Hamiltonian and forced damped system, are symmetric in a sense that the successive impacts for each particle are divided by half-period intervals, and absolute amounts of momentum transferred to given particle in the course of given impact is the same. From the above equation, it is easy to derive the matrix, that describes the evolution of perturbed phase trajectory between two successive impacts:

$$L = \exp\left(\frac{\pi}{\omega} A\right) \quad (51)$$

To describe the evolution of the perturbed phase trajectory in the course of impacts, we apply a formalism of saltation matrix [25]. Since the impacts are instantaneous independent events, they can be treated separately and then combined to result in following saltation matrix:

$$S = \begin{bmatrix} \tilde{S}_{(N+1) \times (N+1)} & 0_{(N+1) \times (N+1)} \\ \hat{S}_{(N+1) \times (N+1)} & \tilde{S}_{(N+1) \times (N+1)} \end{bmatrix} \quad (52)$$

where

$$\tilde{S} = \begin{bmatrix} 1 - (1+e) \sum_k \delta_{1k} & 0 & \cdots & \cdots & 0 \\ 0 & 1 - (1+e) \sum_k \delta_{2k} & 0 & & \vdots \\ \vdots & 0 & \ddots & \ddots & \vdots \\ \vdots & & \ddots & 1 - (1+e) \sum_k \delta_{(N-1)k} & 0 \\ 0 & \cdots & \cdots & 0 & 1 \end{bmatrix} \quad (53)$$

$$\hat{S} = \begin{bmatrix} \frac{(1+e) \sum_k \delta_{1k} \psi_k}{\Gamma_1} & 0 & \cdots & \cdots & 0 \\ 0 & \frac{(1+e) \sum_k \delta_{2k} \psi_k}{\Gamma_2} & 0 & & \vdots \\ \vdots & 0 & \ddots & \ddots & \vdots \\ \vdots & & \ddots & \frac{(1+e) \sum_k \delta_{(N-1)k} \psi_k}{\Gamma_{N-1}} & 0 \\ 0 & \cdots & \cdots & 0 & 1 \end{bmatrix} \quad (54)$$

with $\psi_k = \ddot{u}_k(\phi-)$ and $\Gamma_k = p_k$ for the hamiltonian model, and $\psi_k = \ddot{v}_k(\phi-)$ and $\Gamma_k = \Gamma = p + \dot{G}(\phi)$ for the forced-damped model. Note that for the Hamiltonian model the coefficient of restitution e is set to unity.

Due to the symmetry of even functions composing the Fourier series, the monodromy matrix can be written compactly as follows:

$$M = (LS)^2 \quad (55)$$

As it was mentioned above, the eigenvalues of this monodromy matrix are computed numerically for given parameter values. The resulting stability pattern in the space of parameters are exemplified in the next section.

V. NUMERIC VALIDATION AND STABILITY PATTERNS

A. Hamiltonian Model

In order to assess the properties of the analytic solution, and to verify the accuracy of numeric algorithms, we compare the results of the analysis to numeric simulations. The simulations were performed in MatLab; the vibro-impact was modeled according to the impact law using built-in event-driven algorithms with Runge-Kutta (RK) solver. Simulations show that the analytic solutions perfectly coincide with the numeric results. Fig. 1 demonstrates that, as one would expect, if the DB is exponentially localized, it looks very similar both for very short and very long chains.

When considering the MBs, there are two possible states for each site – in-phase or out-of-phase with respect to the 0-th mass. Both options in the case of 2-site DB are presented in Fig. 2. Due to the symmetry, when the two sites are in anti-phase, the sum of the two forces applied to the mass between them is zero, i.e the mass is in complete halt. Besides this phenomenon, the localization appears to be similar; however, the other masses are in opposite phases as seen in Fig. 3.

While the MB has only two sites, the formation is necessarily symmetric and therefore the displacement of the

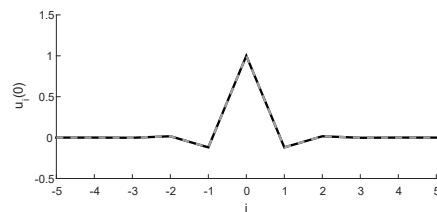


FIG. 1: Comparison of the displacement amplitude of the particles between $N = 10$ (black) and $N = 300$ (dashed gray) with a single site DB. Negative indices denotes the i -th mass in the chain where $i = N + 1 +$ (negative index) to better represent the periodic boundary condition.

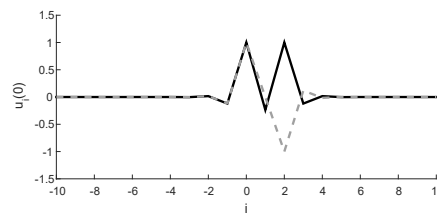


FIG. 2: Comparison of the displacement amplitude of the particles between in-phase (black) and anti-phase (dashed gray) 2-site MB. Negative indices denotes the i -th mass in the chain where $i = N + 1 +$ (negative index) to better represent the periodic boundary condition.

impacting masses remains identical (or inverse if in anti-phase). When there are more than two sites, this symmetry can be broken. The oscillations are still in-phase (or anti-phase), but the impacts are not equivalent, i.e. different particles exchange different amounts of momentum with the constraints in the course of impacts, as demonstrated in Fig. 4.

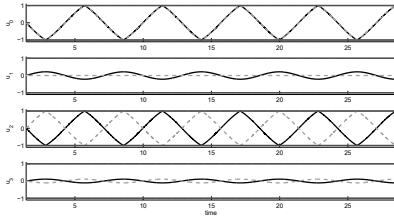


FIG. 3: Comparison of the displacements of the first 4 particles between in-phase (black) and anti-phase (dashed gray) 2-site MB for $N = 20$.

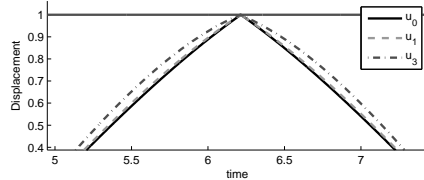


FIG. 4: Displacements of impacting particles for the 3-site MB with excited sites at 0, 1 and 3 for $N = 20$.

B. Forced-Damped Model

In the case of the forced-damped model, the numeric simulations are in accordance with the analytic solution. It is also clear that, unlike the Hamiltonian model where the amplitude rapidly converges to zero as the particle is further away from the localization site, in the forced-damped model it converges as rapidly, but to $G(t)$ instead. Fig. 5 illustrates the difference between the MBs in similar chains with relatively large and small number of particles.

It is difficult to obtain analytic results for the MBs with different phases at different sites, since these solutions are no more symmetric. Thus, they have been found numerically. Fig. 6 shows a simple example of such solution. The difference in velocities clearly indicates the phase differences between the localization sites.

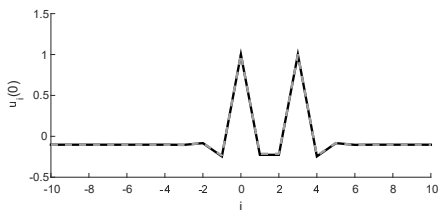


FIG. 5: Comparison of the displacement amplitude of the particles between $N = 20$ (dashed gray) and $N = 300$ (black) with a 2-site MB. Negative indices denote the i -th mass in the chain where $i = N + 1 +$ (negative index) to better represent the periodic boundary condition.

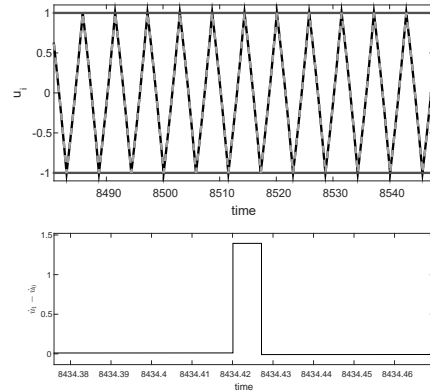


FIG. 6: Top: Displacements u_0 (black) and u_1 (dashed gray) for a Forced 3-site MB with sites at $n = 0, 1, 2$ with $N = 20$. Bottom: The difference in the velocities $\dot{u}_1 - \dot{u}_0$.

C. Stability

The stability analysis can be more easily verified and illustrated in the forced-damped case, since the solutions are hyperbolic dynamical attractors. The analysis reveals two mechanisms of the loss of stability – via pitchfork bifurcation (corresponding to Floquet multipliers leaving the unit circle through positive side of the real axis) and Hopf (Neimark-Sacker) bifurcation which corresponds to a conjugate pair of complex Floquet multipliers leaving the unit circle. Fig. 7 shows the existence-stability map for the two-site multi-breather in the plane of $\omega - \gamma_2$ where both possible bifurcation scenarios are present. The MB solution ceases to exist if the frequency crosses the boundary of the propagation zone, or if some particle achieves the grazing limit. The latter restriction means that either the displacement of one of the “non-impacting” particles approaches unity, or the amount of momentum transferred to the “impacting” particle approaches zero. In both cases, the solution can remain localized, but should be re-derived due to modification of the subset of the “impacting” particles. Fig. 8 presents the examples of the DBs for sets of parameters in the stable and unstable zones.

As it was mentioned before, there are two mechanisms for the loss of stability. One can gain some insight into physical reasons for the loss of stability by inspection of the corresponding eigenvectors of the monodromy matrix. For the pitchfork bifurcation, Fig. 9 shows strongly localized eigenvector. Furthermore, the localization is at the MB sites and appears to be anti-symmetric. This means that the bifurcation leads to breaking of the symmetry. By slow “sweeping” the frequency from the stable regime to the unstable, the new branch created by the pitchfork bifurcation can be traced, and the asymmetric MB appears as presented in Fig. 10

For the case of Neimark - Sacker bifurcation, Fig. 7 demonstrates peculiar structure for the stability boundary with multiple “wells”. Computation of the eigenvectors

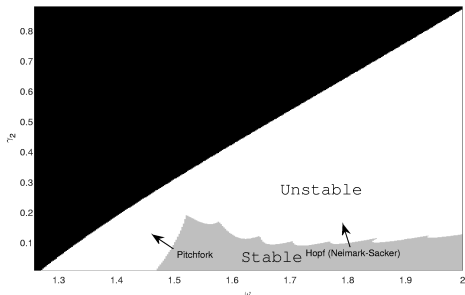


FIG. 7: Existence-stability map for a 2-site Forced MB with sites at 0 and 1 for $N = 20$, $\gamma_1 = 0.1$, $e = 0.9$ and $A = 1.5$. In the black zone the DB solution with the considered structure does not exist.

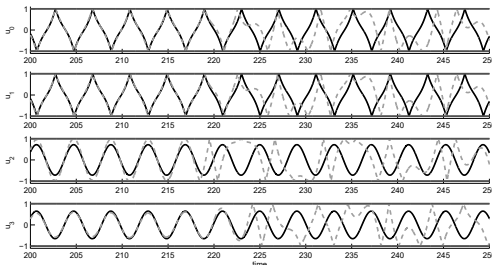


FIG. 8: Analytic prediction (black) and numerical approximation (dashed gray) of the displacements of the first 4 masses for the unstable forced DB.

tors responsible for the loss of stability on the boundaries of these wells reveals that each well is related to different spatial mode of the loss of stability. Examples of these modes are presented in Fig. 11. While the part corresponding to the velocity is mostly localized at the MB sites, the part corresponding to the displacements is not localized, and apparently depends on the number of particles in the chain fragment.

From Fig. 11 it is clear, that sharp differences between the neighboring wells occur due to the fact that the chain

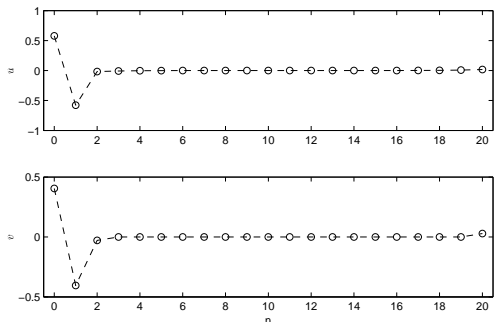


FIG. 9: Values of a typical eigenvector corresponding to the pitchfork bifurcation for the 2-site forced MB with excitation sites at 0 and 1. u and v denote displacements and velocity components of the eigenvectors respectively.

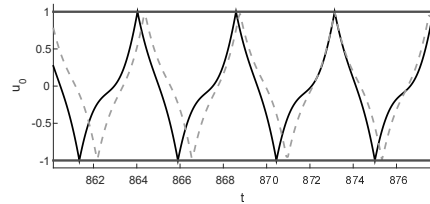


FIG. 10: Analytic prediction for the symmetric solution (dashed gray) and numerical simulation (black) of the displacement of the impacting particle for $N = 20$ and $\gamma_2 = 0.07$ with the 2-site forced MB after breaking of the symmetry.

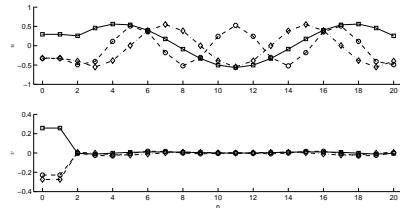


FIG. 11: Spatial profiles of several eigenvectors corresponding to Neimark-Saker bifurcation for the 2-site forced MB with sites at 0 and 1. u and v denote displacements and velocity components of the eigenvectors respectively. Square marker, diamond marker and circle marker correspond to the first, the second and the third “well” from the left respectively.

is relatively short, so there is big difference between lower eigenmodes. So, one can conjecture profound “well structure” for the stability boundary of the MBs in relatively short chains, and transition to smooth boundaries for longer chains. Fig. 12 confirms this conjecture and reveals clear correlation between the number of particles and the number of the wells. It also comes to explain why this peculiar structure was not observed in previous works. The wells become smaller and more dense as the number of particles increases. It is also interesting to note that the structure of the “pitchfork” fragment of the stability boundary does not seem to be significantly affected by the number of particles. This is understandable, since the corresponding eigenvector in all explored cases is strongly localized at the DB site.

The stability of the Hamiltonian model is more difficult for numeric verification, since the solutions are not attractors. However, interesting data may be procured from it, especially with respect to appearance of unstable Floquet multipliers with non-zero imaginary part. In Fig. 13 the loss of stability occurs through the Neimark-Saker bifurcation is shown together with the approximation of the border line. One can thus conjecture that the Hopf bifurcation occurs due to interaction with the boundary of the propagation zone.

The analytic result shows that the solution converges to that of the infinite chain as the size of the system grows. The numerics shows that the existence-stability map appears to be very similar regardless the system

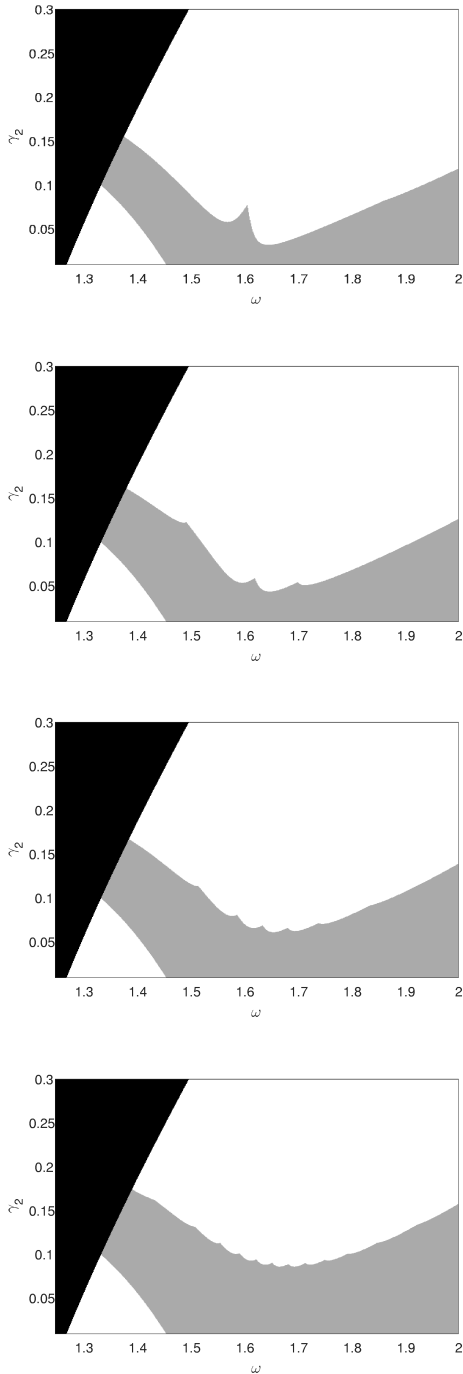


FIG. 12: Stability map for the single-site DB with $\gamma_1 = 0.1$, $e = 0.9$ and $A = 1.5$ for (a) $N = 5$ (b) $N = 10$ (c) $N = 20$ (d) $N = 40$ (top-down)

size. In Fig. 14 we demonstrate that any noticeable modifications of the stability boundary occur only for extremely short chains with $N = 3 - 4$. This is very different from the stability patterns observed for the forced-damped case. Corresponding eigenvector turns out to be strongly localized, as presented in Fig. 15.

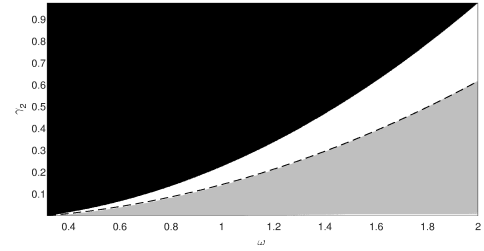


FIG. 13: Existence - stability map for the single-site conservative DB for $N = 20$ and $\gamma_1 = 0.1$. The dashed line corresponds to $\omega^2 = \gamma_1 + (19/3)\gamma_2$

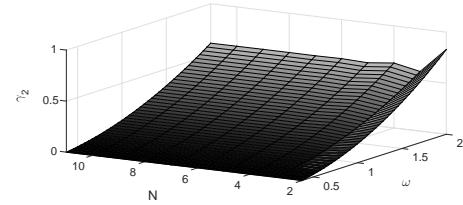


FIG. 14: Evolution of the stability boundary of the single-site DB in the frequency-stiffness domain as a function of the system size.

In addition to the system size, it is also interesting to examine the effect of the proximity between the localization sites for the MB solution. One would expect its influence to vanish very quickly as the distance between the sites increases, due to the strong localization; it is indeed the case as shown in Fig. 16. However, one should note that the proximity has a very strong influence when the localization sites are close.

Moreover, in the case of the conservative MBs the eigenvectors corresponding to the loss of stability also could be delocalized. In Fig. 17 we demonstrate the stability diagram for the two-site anti-phase multi-breather. This diagram demonstrates an interesting pattern of thin stability strips, each boundary corresponding to the Neimark-Saker bifurcation with different eigenvectors, as shown in Fig. 18. This structure exhibits strong depen-

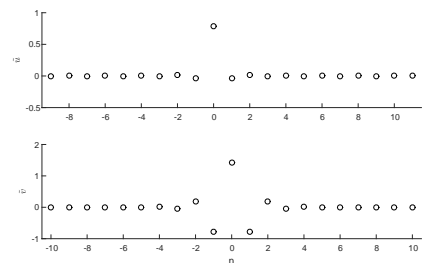


FIG. 15: Shape of eigenvector corresponding to the Neimark-Saker bifurcation for the single-site conservative DB shown in Fig. 13. \tilde{u} and \tilde{v} denote displacements and velocity components of the eigenvector respectively.

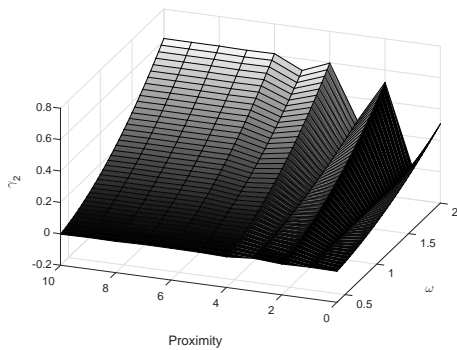


FIG. 16: Evolution of the loss of stability boundary of the 2-site MB in the frequency-stiffness domain as a function of distance between the excited sites (value 0 corresponds to two consecutive excited sites).

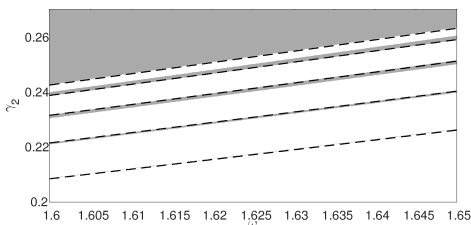


FIG. 17: Stability map for the 2-site MB with excitation sites at 0 and 2 in anti-phase for $N = 20$ and $\gamma_1 = 0.1$.

dence on the number of particles in the chain fragment, similar to the case of the forced-damped DBs.

VI. CONCLUDING REMARKS

The results presented above demonstrate, first of all, that one can analytically derive the exact solutions for the MBs and further explore their existence/stability patterns in the space of parameters with moderate computational efforts. The procedure also revealed certain complications, absent in the case of the single-site DBs. For instance, in order to study the phase differences between various localization sites, one should relax the symmetry conditions and explore more generic families of the periodic localized solutions. Such undertaking would be a natural extension of current study.

Another interesting finding is strong dependence of the stability boundary for the Neimark-Saker bifurcation scenario, and lack of such dependence - for the pitchfork bifurcation. This study used periodic boundary conditions. In the real experiments, with free or fixed boundary conditions, one should expect significant dependence of the breather stability not only on the system size, but also on the proximity of the breather to the system boundary. This point also requires additional exploration.

Acknowledgments

The authors are very grateful to Israel Science Foundation (grant 838/13) for financial support.

-
- [1] S. Flach and C. Willis, *Physics Reports* **295**, 181 (1998), ISSN 0370-1573.
- [2] S. Flach and A. V. Gorbach, *Physics Reports* **467**, 1 (2008), ISSN 0370-1573.
- [3] A. F. Vakakis, L. I. Manevitch, Y. V. Mikhlin, V. N. Pilipchuk, and A. A. Zevin, *Normal modes and localization in nonlinear systems* (Springer, 1996).
- [4] D. K. Campbell, *Nature* **432**, 455 (2004).
- [5] A. F. Vakakis, O. V. Gendelman, L. A. Bergman, D. M. McFarland, G. Kerschen, and Y. S. Lee, *Nonlinear targeted energy transfer in mechanical and structural systems*, vol. 156 (Springer Science & Business Media, 2008).
- [6] P. W. Anderson, *Phys. Rev.* **109**, 1492 (1958).
- [7] C. Pierre and E. Dowell, *Journal of Sound and Vibration* **114**, 549 (1987), ISSN 0022-460X.
- [8] O. Bendiksen, *Chaos, Solitons & Fractals* **11**, 1621 (2000), ISSN 0960-0779.
- [9] E. Trias, J. J. Mazo, and T. P. Orlando, *Phys. Rev. Lett.* **84**, 741 (2000).
- [10] N. Lazarides, M. Eleftheriou, and G. P. Tsironis, *Phys. Rev. Lett.* **97**, 157406 (2006).
- [11] L. Q. English, F. Palmero, P. Candiani, J. Cuevas, R. Carretero-González, P. G. Kevrekidis, and A. J. Sievers, *Phys. Rev. Lett.* **108**, 084101 (2012).
- [12] *Journal of Sound and Vibration* **329**, 3835 (2010), ISSN 0022-460X.
- [13] M. Kimura and T. Hikiyama, *Physics Letters A* **373**, 1257 (2009), ISSN 0375-9601.
- [14] E. Kenig, B. A. Malomed, M. C. Cross, and R. Lifshitz, *Phys. Rev. E* **80**, 046202 (2009).
- [15] M. Sato, S. Imai, N. Fujita, S. Nishimura, Y. Takao, Y. Sada, B. E. Hubbard, B. Ilic, and A. J. Sievers, *Phys. Rev. Lett.* **107**, 234101 (2011).
- [16] M. Sato, B. E. Hubbard, and A. J. Sievers, *Rev. Mod. Phys.* **78**, 137 (2006).
- [17] A. Trombettoni and A. Smerzi, *Phys. Rev. Lett.* **86**, 2353 (2001).
- [18] O. V. Gendelman and L. I. Manevitch, *Phys. Rev. E* **78**, 026609 (2008).
- [19] J. Cuevas, L. Q. English, P. G. Kevrekidis, and M. Anderson, *Phys. Rev. Lett.* **102**, 224101 (2009).
- [20] O. V. Gendelman, *Phys. Rev. E* **87**, 062911 (2013).
- [21] M. J. Ablowitz and J. F. Ladik, *Journal of Mathematical Physics* **17**, 1011 (1976).
- [22] A. A. Ovchinnikov and S. Flach, *Phys. Rev. Lett.* **83**, 248 (1999).
- [23] N. Perchikov and O. Gendelman, *Physica D: Nonlinear Phenomena* **292-293**, 8 (2015), ISSN 0167-2789.
- [24] S. Strogatz, *Nonlinear Dynamics and Chaos: With Applications to Physics, Biology, Chemistry, and Engineering*

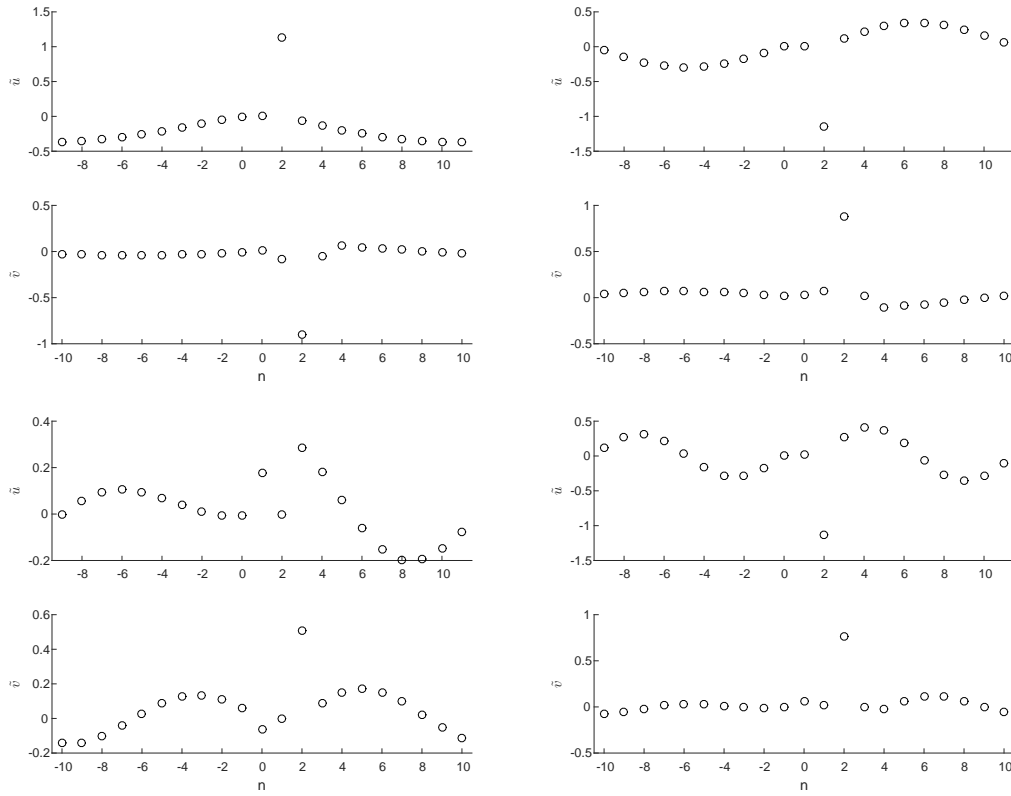


FIG. 18: Shapes of selected eigenvectors corresponding to Neimark-Saker bifurcation for a 2-site MB with $N = 20$ and sites at 0 and 2 in anti-phase corresponding to loss of stability stripes from the top down in fig. 17 (left-to-right, top-to-bottom)

ing, Advanced book program (Westview Press, 1994), ISBN 9780738204536.

[25] M. H. Fredriksson and A. B. Nordmark, Proceedings of

the Royal Society of London A: Mathematical, Physical and Engineering Sciences **456**, 315 (2000), ISSN 1364-5021.